The Journal of Immunology

Chemical Attenuation of *Plasmodium* in the Liver Modulates Severe Malaria Disease Progression

Matthew D. Lewis, Jochen Behrends, Cláudia Sá e Cunha, António M. Mendes, Felix Lasitschka, Julia M. Sattler, Kirsten Heiss, Taco W. A. Kooij, Miguel Prudêncio, Gerhard Bringmann, Friedrich Frischknecht and Ann-Kristin Mueller

J Immunol 2015; 194:4860-4870; Prepublished online 10 April 2015;
doi: 10.4049/jimmunol.1400863
http://www.jimmunol.org/content/194/10/4860

The Journal of Immunology is published twice each month by The American Association of Immunologists, Inc., 9650 Rockville Pike, Bethesda, MD 20814-3994.

Print ISSN: 0022-1767 Online ISSN: 1550-6606.

Chemical Attenuation of *Plasmodium* in the Liver Modulates Severe Malaria Disease Progression

Matthew D. Lewis,*,† Jochen Behrends,‡ Cláudia Sá e Cunha,§ António M. Mendes,§ Felix Lasitschka,†,¶ Julia M. Sattler,* Kirsten Heiss,*,‖ Taco W. A. Kooij,#, Miguel Prudêncio,§ Gerhard Bringmann,†† Friedrich Frischknecht,* and Ann-Kristin Mueller*,†**

Cerebral malaria is one of the most severe complications of malaria disease, attributed to a complicated series of immune reactions in the host. The syndrome is marked by inflammatory immune responses, margination of leukocytes, and parasitized erythrocytes in cerebral vessels leading to breakdown of the blood–brain barrier. We show that chemical attenuation of the parasite at the very early, clinically silent liver stage suppresses parasite development, delays the time until parasites establish blood-stage infection, and provokes an altered host immune response, modifying immunopathogenesis and protecting from cerebral disease. The early response is proinflammatory and cell mediated, with increased T cell activation in the liver and spleen, and greater numbers of effector T cells, cytokine-secreting T cells, and proliferating, proinflammatory cytokine-producing T cells. Dendritic cell numbers, T cell activation, and infiltration of $CD8^+$ T cells to the brain are decreased later in infection, possibly mediated by the anti-inflammatory cytokine IL-10. Strikingly, protection can be transferred to naive animals by adoptive transfer of lymphocytes from the spleen at very early times of infection. Our data suggest that a subpopulation belonging to $CD8^+$ T cells as early as day 2 postinfection is responsible for protection. These data indicate that liver stage–directed early immune responses can moderate the overall downstream host immune response and modulate severe malaria outcome. *The Journal of Immunology*, **2015, 194: 4860–4870.**

Human cerebral malaria (HCM) is a lethal complication of *Plasmodium falciparum* infection, causing unrousable coma marked by the plugging of cerebral capillaries with parasitized erythrocytes (pRBCs) and margination of monocytes and macrophages within cerebral vessels (1, 2). Cerebral pathology does not occur until several days or weeks postinfection, after the parasite has passed through the obligatory liver phase, egressed, and established a blood infection by invading erythrocytes. The late onset of severe symptoms means that patients with HCM typically do not present in a clinical setting until the onset of fulminant disease, rendering the pre-erythrocytic and early stages of disease development largely unknown. Furthermore, because of limitations inherent in study of human subjects, the precise mechanisms of HCM immunopathogenesis have not been extensively described.

By using susceptible mouse strains, it is possible to study the early events that lead to cerebral pathology. Infection of C57BL/6 mice with *Plasmodium berghei* ANKA mimics human symptoms and is arguably the best murine model for this disease complication, termed experimental cerebral malaria (ECM) (3). It has been demonstrated in this model that cerebral pathology is caused by a complicated systemic inflammatory Th1 response involving both innate and adaptive cellular immunity, and a crucial role for both parasitemia and parasite Ag presentation has been demonstrated (4). This response involves the induction of proinflammatory cytokines, such as IFN-γ and lymphotoxins, activation of monocytes, macrophages, and neutrophils, and the chemotaxis of the latter two to the brain. Subsequently, $CD8^+$ T cells migrate to the cerebral tissues in a largely Ag-specific manner. This migration is caused by an increased APC-mediated priming of T lymphocytes at the spleen and by an upregulation of MHC class I (MHCI), MHCII, and two endothelial receptors, ICAM-1 and VCAM-1 (3). These events cause blood–brain barrier (BBB) disruption, perhaps due to $CD8^+$ T cell–mediated cytolysis of the brain microvessels that are cross-presenting parasite Ag (5), ultimately leading to hemorrhaging, neuronal disturbance, coma, and death (6–8).

In HCM, parasite attenuation may alter the outcome of severe pathology. It has been proposed that sulfadoxine-pyrimethamine administration may generate low-dose blood-stage inocula and attenuate infection kinetics and pathology (9, 10). Certainly, other forms of parasite attenuation have been used to generate vaccine-like immunity against malaria in ECM mouse models. For example, attenuation of *Plasmodium* sporozoites by radiation, gene knockout, and drug treatment leads to the developmental arrest of liver stages (exoerythrocytic forms or EEFs) and causes vaccine-like sterilizing protection to subsequent wild-type challenge. This protection is thought to be mediated predominantly by $CD8^+$

*Centre for Infectious Diseases, Parasitology Unit, Heidelberg University Hospital, D 69120 Heidelberg, Germany; †German Centre for Infection Research, D 69120 Heidelberg, Germany; ‡Core Facility Fluorescence Cytometry, Research Center Borstel, D 23845 Borstel, Germany; §Instituto de Medicina Molecular, Faculdade de Medicina, Universidade de Lisboa, 1649-028 Lisbon, Portugal; ¶Institute of Pathology, Heidelberg University Hospital, D 69120 Heidelberg, Germany; ‖MalVa GmbH, D 69121 Heidelberg, Germany; #Department of Medical Microbiology, Radboud Institute for Molecular Life Sciences, Radboud University Medical Centre, 6500 HB Nijmegen, the Netherlands; **Centre for Molecular and Biomolecular Informatics, Radboud Institute for Molecular Life Sciences, Radboud University Medical Centre, 6500 HB Nijmegen, the Netherlands; and ††Institute for Organic Chemistry, University of Würzburg, 97074 Würzburg, Germany

Received for publication April 7, 2014. Accepted for publication March 11, 2015.

Address correspondence and reprint requests to Dr. Ann-Kristin Mueller, University Hospital Heidelberg, Centre for Infectious Diseases, Parasitology Unit, Im Neuenheimer Feld 324, D 69120 Heidelberg, Germany. E-mail address: ann-kristin.mueller@uni-heidelberg.de

The online version of this article contains supplemental material.

Abbreviations used in this article: BBB, blood–brain barrier; CAT, chemical attenuation treatment; *Ct*, cycle threshold; DC, dendritic cell; ECM, experimental cerebral malaria; EEF, exoerythrocytic form; HCM, human cerebral malaria; MHCI, MHC class I; NCM, negated cerebral malaria; pRBC, parasitized erythrocyte; qRT-PCR, quantitative RT-PCR.

T cells (11–13). However, parasite attenuation has not yet been extensively examined in the context of cerebral malaria, despite evidence that it may afford some protection. For example, in humans, a malaria vaccine candidate, RTS,S, has been shown to cause partial protection against severe and cerebral malaria, possibly because of impairment of infectious merozoite release by infected liver cells (14–16). Furthermore, in the mouse model, it has previously been demonstrated that antimalarial treatment of infected mice just before the onset of ECM symptoms, the usual end point of infection, attenuates infection by decreasing parasitemia and delaying the onset of cerebral pathology (4).

Few studies have examined the pre-erythrocytic stage or the interaction of immune responses between liver and blood that occurs in early infection on the immunopathogenesis of ECM. Some initial work recently indicated a potential role for the liver stage in modulation of disease severity, with impaired liver-stage development and merozoite formation correlating with a reduced incidence of cerebral pathology in a transgenic parasite lacking a *Plasmodium*-specific apicoplast protein (17). However, unlike vaccine-like sterilizing immunity induced by attenuated strains, few studies have examined very early cellular immune responses associated with parasite attenuation and their roles in protection from cerebral pathology. One study demonstrated a correlation between protection from cerebral pathology and increased β_2-microglobulin–specific IFN-γ production at 24 h postinfection (18). The authors hypothesized that $CD8^+$ T cells were the source of the IFN-γ. A subsequent study demonstrated that when irradiated blood-stage parasites were administered as a vaccine, ECM did not develop upon further challenge with normal parasites (19). Similarly, protected animals produced early IFN-γ, which the authors hypothesized is produced by splenic lymphocytes.

We investigated the role of early immune responses and protection from cerebral malaria in the context of attenuating parasite infection. In doing so, we developed a reproducible model for attenuating the malarial liver stage as a means of manipulating the host immune response to alter the clinical outcome of ECM. We propose that this model causes modulation of cerebral disease by the induction of $CD8^+$ T cell responses earlier than it would occur in natural infection, causing deregulation of downstream, systemic Th1 responses and reduced $CD8^+$ T cell priming.

Materials and Methods

Ethics statement

All animal experiments were performed according to European regulations concerning FELASA category B and GV-SOLAS standard guidelines. Animal experiments were approved by German authorities (Regierungspräsidium Karlsruhe, Germany), § 8 Abs. 1 Tierschutzgesetz (TierSchG) under the license G-6/09 ("MALBI: Malaria Biologie und Immunologie" ["The Biology and Immunology of Malaria"]). For all experiments, C57BL/6 mice were purchased from Janvier, France, and kept under specified pathogen-free conditions within the animal facility at Heidelberg University (Interfacultary Biomedical Facility). IL-$10^{tm1Cgrn}$ knockout mice were a kind gift from the University of Bonn, Bonn, Germany. Animals were matched for sex and age.

Plasmodium *life cycle and rodent methods*

Anopheles stephensi mosquitoes infected with *P. berghei* ANKA cl15cy1 (MR4) or *P. berghei* ANKA 676m1cl1 (Pb GFP-Luc_{con}; a kind gift from Andrew Waters, Glasgow, U.K.) (20) were kept under defined conditions of 80% humidity and 21°C. Sporozoites were dissected from mosquito salivary glands at days 17–24 postinfection. Isopentaquine (N1-isopropyl-N4-(6-methoxyquinolin-8-yl)-pentane-1,4-diamine) was kindly provided by Gerhard Bringmann (University Würzburg, Würzburg, Germany). The compound was dissolved in 1× PBS with 5% Cremophor RH 40 (BASF, Ludwigshafen, Germany) and administered to groups of mice by s.c. injection of 30 mg/kg at days −2, −1, and 0. A total of 10,000 infectious salivary gland sporozoites were inoculated at day 0 by i.v. injection into the tail vein. Parasitemia was monitored by daily blood smear and Giemsa stain.

Rapid and sensitive detection of blood-stage parasites from tail blood by PCR

For the rapid and sensitive detection of the presence of *P. berghei* blood-stage parasites in the peripheral blood after the completion of the liver-stage development, we developed a simple and fast PCR-based method. At the indicated time points, 10 μl tail blood was collected in 500 μl Alsever's solution or PBS and cells were collected by centrifugation for 5 min at 1800 rpm. Erythrocytes were lysed in 500 μl 0.1% saponin in PBS and free parasites collected by centrifugation for 5 min at 8000 rpm. Cells were washed once with 500 μl PBS and collected by centrifugation for 5 min at maximum speed. The pellet was taken up in ∼20 μl ddH_2O and snap-frozen for at least 5 min at −80°C and kept frozen until used for PCR detection. Parasites were detected with primers specific for 18S rRNA (Forward 5′-AAGCATTAAATAAAGCGAATACATCCTTAC-3′ and Reverse 5′-GGAGATTGGTTTTGACGTTTATGTG-3′) using a 10-min 94°C hot start PCR protocol.

Rapid Murine Coma and Behavior Scale

As described previously (21), animals were assessed for 10 parameters of cerebral symptoms, such as coordination and motor performance, and scored 0–2, where a 0 score correlates with lowest function and 2 the highest. Animals were assessed daily and scored from 0 to 20 according to this scale.

Cytokine bead array analysis

Cytokine bead array analysis was performed as previously described using a Th1/Th2/Th17 CBA kit (BD Biosciences). For analysis of cytokine concentration, organ homogenates were isolated at the designated time point postinfection. In brief, liver was gently pressed through a sieve, then washed with 1× PBS containing 1% FCS and 2 mM EDTA and centrifuged (10 min, 1500 rpm). Supernatants were taken for cytokine analysis and stored at −20°C in protease inhibitor mixture (1× protease inhibitor [Roche], 0.05% Tween 20 in PBS) until needed. Organ homogenates and serial dilutions of cytokine standards were incubated with 50 μl beads diluted in dilution buffer. PE-detection reagent mix was added and samples were incubated for 2 h in the dark. Samples were subsequently washed in wash buffer; 300 events/cytokine were acquired on a FACSCalibur, and gating on the total bead population identified by a forward scatter-side scatter profile. Cytokine concentrations were analyzed by FCAP Array software (BD Biosciences).

Flow cytometry

For flow-cytometry analysis, mice were sacrificed and perfused intracardially with 1× PBS. Organs were prepared as single-cell suspensions via homogenization through a 70-μm cell strainer in PBS. Liver lymphocytes were isolated by resuspension in 33% Percoll and collection in the cell pellet after centrifugation at 2000 rpm. Cells were then subjected to erythrocyte lysis in erythrocyte lysis buffer (0.037 g EDTA, 1 g $KHCO_3$, 8.26 g NH_4Cl in 1 L ddH_2O, pH 7.4). Cells were then washed and counted in a hemocytometer. For T cell cytokine analysis, cells were stimulated ex vivo with 1 μM ionomycin (Sigma-Aldrich) and 50 ng/ml PMA (Sigma-Aldrich) with 10 μg/ml brefeldin A to inhibit Golgi function for 5 h at 37°C. Afterward, and where cells were not stimulated, cells were stained and analyzed for expression of CD8a (clone 53-6.7/PerCP; BD Biosciences), CD4 (clone GK1.5/FITC; eBioscience), CD44 (clone IM7/allophycocyanin; BD Biosciences), CD62L (clone MEL-14/PE; BD Biosciences), CD25 (clone PC61.5/allophycocyanin; eBioscience), and CD69 (clone H1.2F3/PE-Cy7; eBioscience) markers. For intracellular staining, after surface staining, cells were fixed in 2% PFA, washed, permeabilized with 0.2% saponin lysis buffer, and stained for intracellular cytokines TNF-α (clone MP6-XT22/allophycocyanin; eBioscience), IFN-γ (clone XMG1.2/FITC; eBioscience), and IL-2 (clone JES6-5H4/PE; eBioscience) or included matched isotype controls as appropriate. Data were collected on a FACSCanto and analyzed by CellQuest Pro software (BD Biosciences) or FCS Express (De Novo Software). Brain leukocyte isolation was conducted by cutting brains into pieces and digesting in 0.5 mg/ml collagenase A (Sigma-Aldrich) at 37°C for 30 min. Organs were subsequently passed through a sieve to obtain a single-cell suspension. Cells were pelleted and resuspended in 3 ml 30% Percoll underlaid by 3 ml 37% and 3 ml 70% Percoll. Cells were centrifuged at 2000 rpm for 20 min at room temperature, and cells were collected from the interphase.

Evans blue quantification

Quantification of vascular leakage was performed as described previously (22). In brief, mice were injected i.v. with 150 μl of 1.5% Evans blue

(Sigma-Aldrich) and sacrificed 2 h later to assess vascular leakage; brains were isolated in formamide and incubated for 48 h at 37°C. Absorbance was measured at 620 nm in an ELISA reader with Evans blue concentration assessed via standard curve starting at 400 mg/ml and expressed as milligram dye per gram of brain tissue.

Quantitative real-time PCR

Quantification of parasite liver loads by quantitative real-time PCR (qRT-PCR) was conducted as previously described (23). In brief, mice were killed 42 h after sporozoite infection and livers were removed, homogenized, and subjected to RNA isolation via the RNeasy kit (Qiagen) with cDNA synthesized by the RETROscript (Ambion) kit as per manufacturer's instructions. qRT-PCR was conducted with the ABI 7500 (Applied Biosystems) and Power SYBR Green PCRMasterMix (Applied Biosystems). Relative liver parasite levels were quantified by determining the mean cycle threshold (*Ct*) value of the parasitic *18S ribosomal subunit* using gene-specific primers (GenInfo Identifier, 160641) (forward: 5′-AAGCATTAAATAAAGCGAATACATCCTTAC-3′; reverse: 5′-GGAGATTGGTTTTGACGTTTATGTG-3′), normalized to the mean *Ct* mouse *GAPDH* values (GenInfo Identifier, 281199965) (forward: 5′-CGTCCCGTAGACAAAATGGT-3′; reverse: 5′-TTGATGGCAACAATCTCCAC-3′). Relative copy numbers were determined via the ΔCt method.

Whole-body bioluminescence imaging

The transgenic *P. berghei* line 676m1cl1 (Pb GFP-Luc$_{con}$) (20) was used for the whole-body imaging procedure. Luciferase activity was visualized through whole-body imaging using an in vivo Imaging System (IVIS 100; Caliper Life Sciences) as previously described (24). In brief, animals were anesthetized using isoflurane and their abdomen shaved. D-Luciferin (Synchem Laborgemeinschaft OHG, Germany) was dissolved in PBS and 2.5 mg/mouse injected i.p. After administration of D-luciferin, bioluminescence imaging was directly acquired with an exposure time of 180 s and analyzed using Living Image 2.50.1 (Xenogen, Hopkinton, MA). Units are expressed as photons per second per centimeter squared per steradian (p/s/cm^2/sr).

Depletion experiments

IL-10R Ab, clone 1B1.3A was purchased from Biolegend and administered i.p. at 250 μg at either day −1 or 5 as indicated and 200 μg daily thereafter until the end point of the experiment. CD8-depleting Ab clone 53-6.7 was purchased from Biolegend and administered 150 μg 3 d before the experiment commencement and every 3 d thereafter until the end point of the experiment. Anti-CD25–depleting Ab clone PC61 was purchased from Biolegend and 250 μg was administered i.p. 8 d before sporozoite inoculation. Anti-CD4–depleting Ab clone GK1.5 purified from hybridoma culture was a kind gift from the University of Bonn, and 300 μg was administered i.p. 1 d before the first isopentaquine shot and every 3 d thereafter.

Histology

Brains were carefully removed immediately after death and snap-frozen in liquid nitrogen. Ten-micrometer-thick coronal sections were cut on a cryotome (Leica Microsystems, Vienna, Austria) and directly mounted onto SuperFrost/Plus slides (Microm International, Walldorf, Germany). Serial sections were stained routinely with H&E (Thermo Fisher Scientific, Waltham, MA) and Giemsa (Thermo Fisher Scientific). Finally, slides were blinded and three randomly selected sections per coronal plane were subjected to histological analysis. Examinations were done on an Olympus BX45 research microscope (Olympus, Tokyo, Japan). For semiquantitative analysis of parasite infiltration, histological sections of organs were scored in a blind manner using the following pathological scores (scores are given in parentheses after each category): 1) perivascular infiltration: no infiltrates (0), mild (<25%; 1), moderate (25–50%; 2), or severe (>50%; 3) infiltration; 2) necrosis/hemorrhage: no (0), mild (1), or severe (2); 3) vessels: free (0), luminal myeloid cells (1), or massive blockage (2); 4) parasitemia: 50 vessels were counted in each brain and the percentage of vessels with infected erythrocytes was scored as follows: no parasitemia (0), mild parasitemia of 25% (1), moderate parasitemia of 26–50% (2), and severe parasitemia >50% (3); and 5) hemozoin deposition: no (0), mild (1), moderate (2), severe (3).

Immunohistochemical staining of liver slices

Liver samples were harvested from ECM and negated cerebral malaria (NCM) mice 42 h postinfection with 10,000 *P. berghei* ANKA cl15cy1 sporozoites and fixed with 4% paraformaldehyde in PBS overnight at 4°C. They were washed and subsequently sliced into 50-μm slices using a Vibratome (VT1000S; Leica). Slices were permeabilized and blocked overnight at 4°C in 0.5% v/v Triton X-100 plus 1% w/v BSA and then incubated in the same solution containing goat anti–*P. berghei* UIS4 (1:750; kindly provided by M. Seabra) and mouse anti–*P. berghei* HSP70 (1:250) for ∼2 h at room temperature. After washing with 1× PBS, slices were incubated with a secondary donkey anti-goat Ab conjugated to Alexa Fluor 488 (1:500; Jackson Immunoresearch Laboratories) and donkey anti-mouse conjugated to Alexa Fluor 555 (1:500) for ∼2 h. Cell nuclei were stained with Hoechst 33258 (Molecular Probes/Invitrogen) and F-actin with Alexa Fluor 660 Phalloidin (Molecular Probes/Invitrogen). Forty nonconsecutive stained liver slices were placed on microscope slides and mounted with 24 × 60-mm coverslips using Fluoromount-G (Southern Biotech). Images were acquired with a Zeiss Axiovert 200M to count and measure EEFs. Numbers of EEFs were normalized to the total liver slice area observed. Illustrative pictures were taken using a Zeiss LSM 510 META Point Scanning confocal microscope. All images were analyzed with ImageJ 1.42b software (National Institutes of Health) (25).

Statistical analysis

Data were tested for normal distributions using the D'Agostino and Pearson omnibus normality test. In two group comparisons, statistical significance was determined using *t* test or the two-tailed Mann–Whitney *U* test, depending on distribution of the data. For three or more group comparisons, statistical significance was determined using a one-way ANOVA, with the Bonferroni post hoc analysis for normally distributed data, or a Kruskal–Wallis test, with Dunn post hoc analysis for nonparametric data. Significant disparity between slopes was determined by linear regression analysis using GraphPad Prism 5 software using calculations equivalent to analysis of covariance as outlined by Zar (26). Asterisks signify degrees of significance: ***$p < 0.001$, **$p < 0.01$, *$p < 0.05$, and ns indicates $p > 0.05$.

Results

Experimental animals subjected to chemical attenuation treatment sustain high parasitemias, die of hyperparasitemia-associated anemia, and do not experience development of ECM

We hypothesized that chemical attenuation of the parasite during its liver-stage development could lead to a change in disease outcome. Therefore, we first administered subtherapeutic doses of isopentaquine, an 8-aminoquinoline with a liver-stage action comparable with that of primaquine (27–29). Primaquine and primaquine derivatives are thought to interfere with the cellular respiration, generation of free radicals, and deregulation of electron transport in liver-resident parasites (30).

By subtherapeutic prophylactic administration of isopentaquine before i.v. infection of 10,000 *P. berghei* ANKA salivary gland sporozoites (Fig. 1A), mice became blood-stage–positive but did not show any typical cerebral symptoms, as measured by the Rapid Murine Coma and Behavior Scale described previously (21), and the onset of patency was delayed by 3–4 d (Fig. 1B and 1C). This NCM outcome was characterized by death from hyperparasitemia-associated anemia at days 25–30 postinfection (Fig. 1B and 1C). To investigate this delay, we subjected mice to chemical attenuation treatment (CAT) and subsequently infected them with luciferase-expressing *P. berghei* ANKA parasites (20, 31). In both ECM wild-type controls and mice subjected to CAT we observed a bioluminescent signal localized to the liver up to 48 h postinfection, correlating with parasite biomass (Supplemental Fig. 1). At 72 h postinfection the signal was disseminated throughout the whole body of the mouse, indicative of some merosomes that are able to establish blood-stage infection having been released from the liver at this time point. However, this parasitemia is submicroscopic. From 72 to 96 h postinfection there was a significant reduction in parasite biomass throughout the whole body in animals subjected to CAT (Fig. 1 and Supplemental Fig. 1D). Furthermore, from 48 h to 72 h postinfection at the point of schizogony and merosome release, and from 72 to 96 h postinfection during blood-stage replication, there was a significant decrease in the rate of biomass growth of 68 and 67% ($p = 0.002$, $p = 0.0005$), respectively, in animals subjected

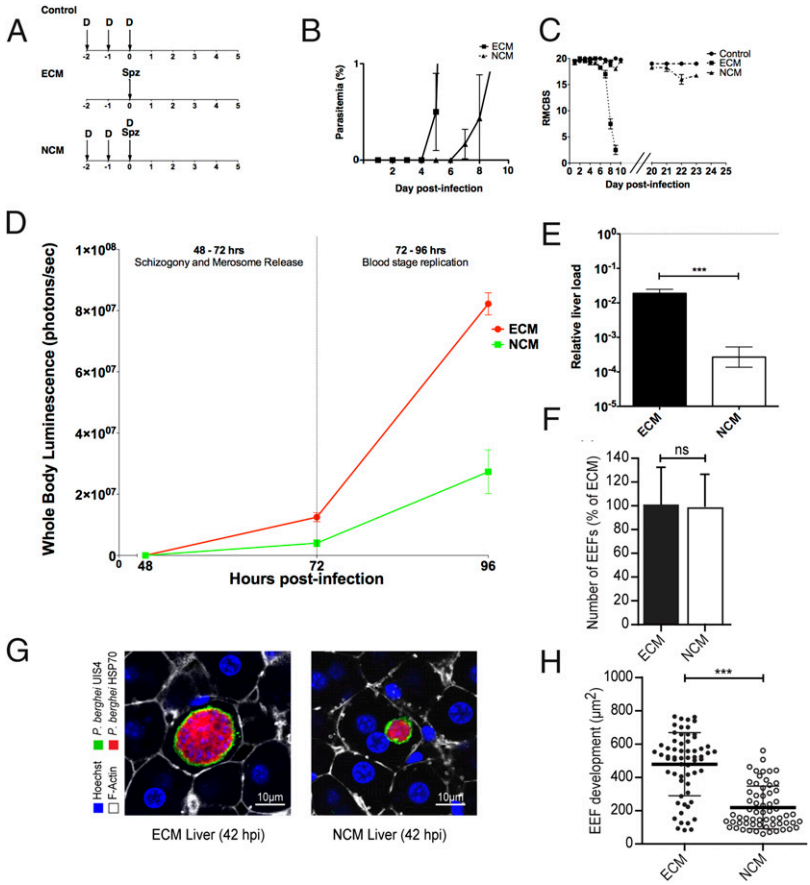

FIGURE 1. CAT attenuates parasite liver development in the liver and blood. (**A**) Schematic representing experimental groups. Animals were subjected to CAT (NCM), and uninfected control mice (Control) were s.c. injected with 30 mg/kg isopentaquine (*D*) at days −2, −1, and 0. Animals subjected to CAT and positive control (ECM) mice were injected i.v. with 10,000 *P. berghei* ANKA salivary gland sporozoites (Spz) at day 0, and chemically attenuated mice (groups of 5 performed in triplicates) were infected with 10,000 *P. berghei* ANKA sporozoites. (**B**) Blood parasitemia in animals subjected to CAT (NCM) and untreated controls (ECM) as determined by blood smear plus Giemsa staining. (**C**) Mouse pathological behavior in animals subjected to CAT (NCM) and untreated controls (ECM) scored from 0 to 20 according to the Rapid Murine Coma and Behavior Scale. (**D**) Animals (groups of 4) were assigned to ECM and NCM groups as described. NCM and ECM mice were infected with 10,000 luciferase-expressing *P. berghei* ANKA sporozoites, and parasite biomass was detected every 24 h in a luminometer after injection of 2.5 mg luciferin. Units are expressed as photons per second per centimeter squared per steradian (p/s/cm^2/sr). (**E**) Animals (groups of 3), assigned as CAT (NCM) and positive control (ECM) mice, were infected with 10,000 *P. berghei* ANKA sporozoites and sacrificed at 42 h postinfection. Livers were extracted and RNA isolated and cDNA synthesized. Relative liver load was calculated via ΔCt analysis based on parasite-specific 18S rRNA transcription. Animals (groups of 4), assigned to chemically attenuated (NCM) and positive control (ECM) mice, were infected with 10,000 *P. berghei* ANKA sporozoites and sacrificed at 42 h postinfection. (**F**) Liver slices were performed and immunofluorescence analysis conducted by staining for *P. berghei* UIS4, *P. berghei* HSP70, Hoechst, and Phalloidin. Number of liver stages was determined in animals subjected to CAT (NCM) and untreated controls (ECM) at 42 h postinfection. (**G**) Representative immunofluorescence images from both samples are presented. (**H**) Size distribution of liver-stage parasites was determined by immunofluorescence analysis in animals subjected to CAT (NCM) and untreated controls (ECM). ***$p < 0.001$. ns, $p > 0.05$.

to CAT (Fig. 1D). The liver stage following CAT was investigated by qRT-PCR analysis of *P. berghei* 18S rRNA transcript levels. Liver-stage development in NCM, characterized by multiple nuclear divisions (32), was decreased as shown by quantitative transcriptional analysis at 48 h postinfection (Fig. 1E). PCR analysis of small volumes of blood (~10 µl) taken every 12 h from mice subjected to CAT and infected with wild-type *P. berghei* ANKA sporozoites revealed a positive parasite signal in NCM animals at 96 h postinfection compared with 84 h postinfection in ECM wild-type control mice (Supplemental Fig. 1B). Liver slices were made, stained, and analyzed by immunofluorescence microscopy at 42 h postinfection, to determine the number and size distribution of liver-stage parasites following CAT (Fig. 1F–H). The number of liver-stage parasites was not significantly different in treated animals compared with untreated controls (Fig. 1F), but hepatic parasite development was found to be significantly inhibited in a vast number of liver-stage parasites in treated animals (Fig. 1G and 1H). A small number of parasites from mice subjected to CAT appeared to be developing normally (Fig. 1H). There was no evidence of loss of integrity of the parasitophorous vacuole in treated mice.

The delay in onset of patent parasitemia, lower liver load, and absence of cerebral symptoms indicate that treatment with isopentaquine leads to an attenuation of liver-stage development and an NCM outcome of malaria infection.

Chemical-attenuation–treated animals do not display signs of cerebral pathology, BBB damage, and parasite sequestration characteristic of ECM pathology

The brain is the centerpiece of ECM pathology. To determine whether mice subjected to CAT were free of the clinical manifestations of ECM within the brain, and not only appearing outwardly healthy, we assessed the brain for indicators of pathology by evaluating the integrity of the BBB and by quantifying the number of infiltrating lymphocytes present in the organ. We injected Evans blue dye at day 8 postinfection, the time point at which control mice

succumbed to cerebral symptoms, to assess the integrity of the vascular endothelium in experimental animals. Upon injection of Evans blue, BBB disruption leads to extravasation of dye into the brain tissue, which can be visualized and assessed quantitatively and qualitatively. Control animals that experienced development of ECM displayed evidence of cerebral pathology—a dark, evenly distributed staining—compared with very faint staining in brains from chemically attenuated NCM animals (Fig. 2A) that was not statistically significantly different from naive brains from noninfected animals by colorimetric analysis (Fig. 2B), indicating that the BBB and vascular endothelium remained intact in animals subjected to CAT. Cryosections of brain tissue were isolated from NCM and ECM mice at the same time point postinfection, and histological analysis revealed no indicators of cerebral damage in the NCM mice, in contrast with the ECM controls, which displayed leukocyte infiltration, parenchymal hemorrhages, subarachnoidal bleeding, and adherence of leukocytes to venule walls (Fig. 2C). NCM mice displayed an intact epithelium, no indicators of subarachnoidal bleeding, and intact blood vessels with no evidence of sequestration (Fig. 2C). ECM is associated with leukocyte sequestration in the brain (33–37), and we accordingly quantified $CD8^+$ and $CD4^+$ T cells infiltrating the brains of ECM and NCM mice. Interestingly, NCM mice showed dramatically fewer $CD8^+$ infiltrates but a comparable number of $CD4^+$ infiltrates (Fig. 2D). This correlates with the observation that $CD8^+$ T cells in the brain-sequestered leukocytes are essential for the cerebral symptoms and mortality in ECM (38). In addition to leukocyte infiltration, protection from cerebral malaria is associated with reduced parasite biomass and sequestration in the brain (39). Thus, we determined the degree of parasite infiltration within the brains of protected and nonprotected mice. Semiquantitative histological analysis of brain sections revealed an approximate 50% reduction in parasite infiltration in NCM mice relative to ECM controls (Fig. 2E).

The host immune response to the liver stage induces protection from ECM

We next examined whether the early host immune response, during which delayed, attenuated liver-stage development occurs, is responsible for the protective phenotype in NCM by parasite transfer experiments. To investigate whether the absence of cerebral pathology in NCM is due to a modification of the parasite at the blood stage, we isolated 10^6 pRBCs from NCM mice and transferred them by i.v. injection into naive animals. All recipient mice displayed clinical symptoms and died of ECM (Fig. 3A and Supplemental Fig. 2), thus indicating that the intraerythrocytic development after CAT remains unaffected and viable in its potential to cause ECM. Furthermore, to determine whether residual antimalarial compound affects the parasite at the blood stage during patency, animals were subjected to CAT and then challenged i.v. with 10^6 or 10^3 pRBCs at either day 5 or 51 h postinfection to mimic the onset of both microscopic and submicroscopic patency in NCM. However, animals were not protected and succumbed to cerebral pathology (Fig. 3B). We therefore assume that an immune response to the very early stages is responsible for the protective phenotype in NCM, and that this prepatent period, during which delayed, attenuated liver-stage development occurs, is crucial for the outcome of ECM.

Overall increase in proinflammatory immune responses in experimental animals subjected to CAT at day 4 postinfection

We dissected the immune response during this period of prepatency 4 d postinfection. We observed a marked increase in total IFN-γ protein in the liver (4286 ± 1100 pg cytokine/g organ) of NCM mice compared with both ECM mice (35.96 ± 6.528 pg cytokine/g organ; $p < 0.005$) and control mice (4.622 ± 0.6982 pg cytokine/g organ; $p < 0.005$, $n = 4$, Mann–Whitney). Because IFN-γ is mainly produced by T lymphocytes and, to a minor extent, by NK and

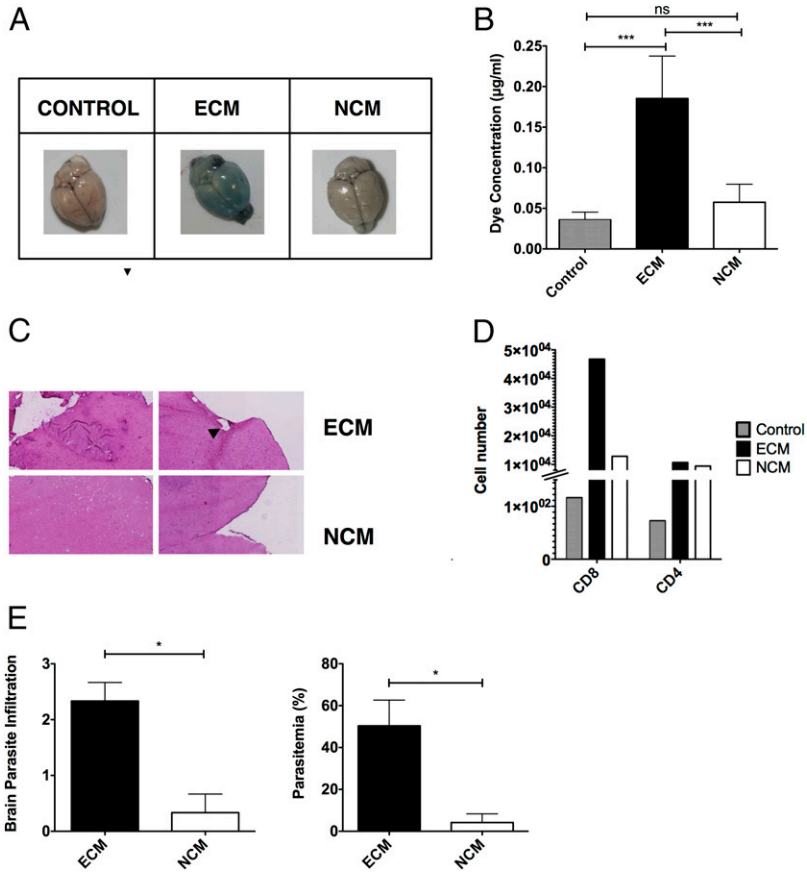

FIGURE 2. Animals subjected to CAT feature absence of pathology and decreased BBB damage. Animals (groups of 5) were assigned to ECM, NCM, and control groups as described and infected with 10,000 *P. berghei* ANKA sporozoites and sacrificed at day 8 postinfection upon the onset of cerebral symptoms. (**A**) Evans blue extravasation in formamide at day 8 postinfection was compared between chemically attenuated and ECM control mice by visual appearance. (**B**) Evans blue extravasation in formamide at day 8 postinfection was compared between chemically attenuated and ECM control mice by measurement of absorbance at 620 nm in comparison with control mice. (**C**) Sections were isolated from brain tissue, stained with H&E, and analyzed for indicators of cerebral pathology. Representative images (*left panels*) display parenchyma and parenchymal hemorrhage, in NCM and ECM groups, respectively, and (*right panels*) subarachnoidal space and subarachnoidal bleeding in NCM and ECM groups, respectively. (**D**) Whole number cerebral $CD8^+$ and $CD4^+$ T cell infiltration at day 8 postinfection was analyzed by flow cytometry. (**E**) Brain parasite infiltration and parasitemia were assessed by histology and scored from 1 to 3, and measured by percentage, respectively. $^{***}p < 0.001$, $^{*}p < 0.05$. ns, $p > 0.05$.

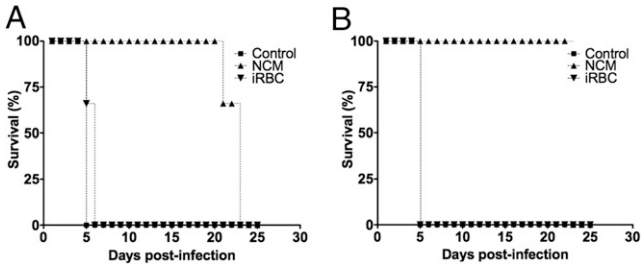

FIGURE 3. The host immune response from the liver induces protection, whereas the pRBC remains pathogenic. (**A**) Mice in the infected RBC (iRBC) group ($n = 5$) were infected with pooled 1×10^6 infected erythrocytes from patent NCM mice ($n = 5$). Survival was tracked. (**B**) Mice in the iRBC group ($n = 5$) were subjected to CAT and at day 5 postattenuation were infected with 1×10^6 infected erythrocytes from pooled infected but untreated mice. Survival was tracked.

NKT cells, we performed flow-cytometry analysis of lymphocytes from liver and spleen tissue followed by intracellular cytokine staining. We observed only a minor difference in the NK cell populations in these organs and no difference in their intracellular cytokine staining (data not shown). However, we observed a pronounced increase in the expression of activation marker CD44 on both $CD8^+$ and $CD4^+$ T cells in the liver and $CD8^+$ T cells in the spleen at day 4 postinfection (Fig. 4). In turn, a higher expression of $CD4^+CD44^{hi}CD62L^-$ effector memory T cells was evident within the liver and decreased numbers of $CD4^+CD44^{hi}CD62L^+$ central memory T cells (Fig. 4A and 4B) were apparent in mice subjected to CAT. Within the spleen, there was a markedly higher number of $CD8^+$ T effector cells in animals subjected to CAT compared with ECM control mice (Fig. 4C and 4D). Intracellular cytokine staining of liver-derived $CD8^+$ and $CD4^+$ T lymphocytes revealed an increased tendency toward IFN-γ^+ cells, in addition to IL-2 and TNF-α at day 4 postinfection (Fig. 5). To assess early T cell activation in NCM, we examined CD69 and CD25 at this time point. We observed a decrease in CD25 and CD69 expression on $CD8^+$ and $CD4^+$ splenic T cells in NCM and none in the liver (Supplemental Fig. 3A–D). CD69 is an early lymphocyte activation marker associated with active, tissue-invading cells (19), whereas CD25 forms part of the IL-2R and has been associated with several cell phenotypes, including early T cell activation (40) and regulatory T cells. These data suggest that early NCM immunopathogenesis

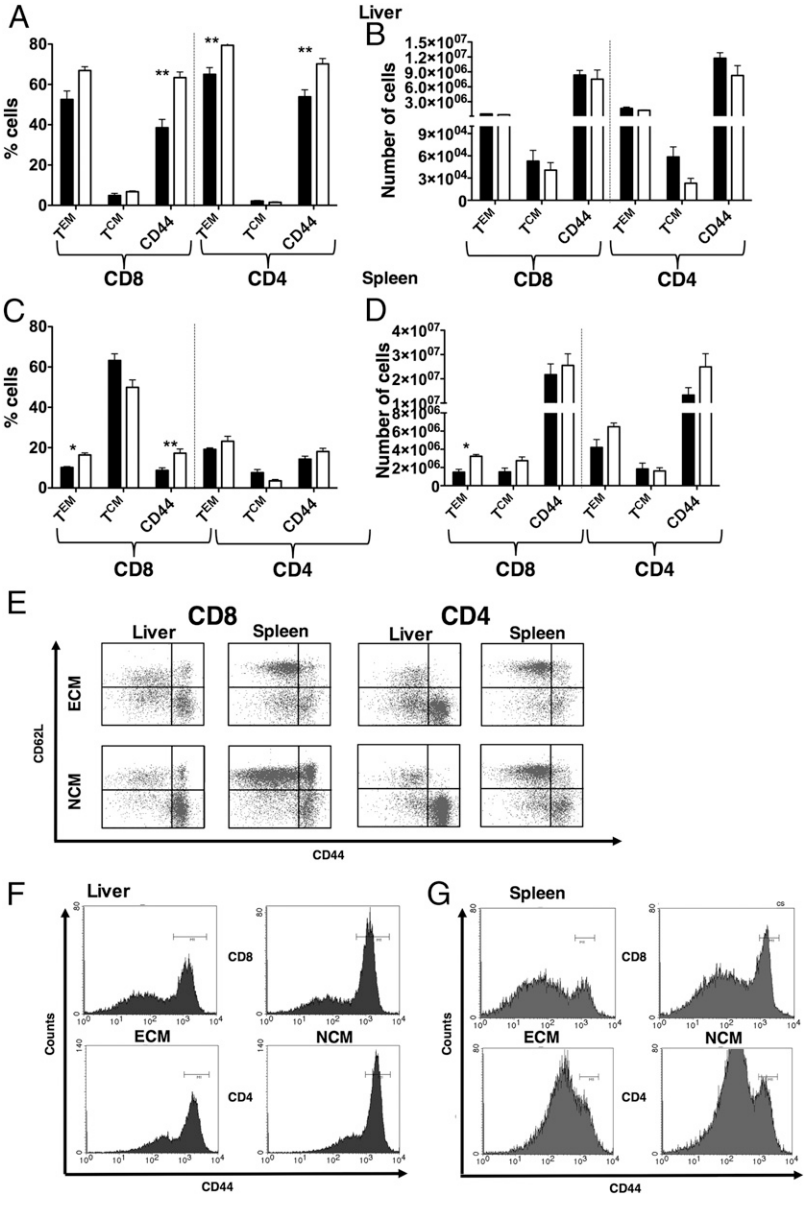

FIGURE 4. Animals subjected to CAT show increased accumulation of activated T cells. Animals (groups of 5) were assigned to ECM, NCM, and control groups as described, and infected with 10,000 *P. berghei* ANKA sporozoites and sacrificed at day 4 postinfection. Additional uninfected control mice were sacrificed. (**A**) Organs were harvested and lymphocytes isolated and stained for CD8, CD4, and activation markers to determine percentage expression of CD8 and CD4 liver effector memory ($CD8^+$ or $CD4^+$ $CD44^{hi}CD62L^-$) and central memory ($CD8^+$ or $CD4^+$ $CD44^{hi}CD62L^+$) cells and percentage of CD8 or CD4-T cells expressing CD44. (**B**) Lymphocytes isolated and stained for CD8, CD4, and activation markers to quantify whole numbers of CD8 and CD4 liver effector memory ($CD8^+$ or $CD4^+$ $CD44^{hi}CD62L^-$) and central memory ($CD8^+$ or $CD4^+$ $CD44^{hi}CD62L^+$) cells and total numbers of CD8 or CD4-T cells expressing CD44. (**C**) Lymphocytes isolated and stained for CD8, CD4, and activation markers to determine percentage expression of CD8 and CD4 splenic effector memory ($CD8^+$ or $CD4^+$ $CD44^{hi}CD62L^-$) and central memory ($CD8^+$ or $CD4^+$ $CD44^{hi}CD62L^+$) cells and percentage of CD8 or CD4-T cells expressing CD44. (**D**) Lymphocytes isolated and stained for CD8, CD4, and activation markers to quantify whole numbers of CD8 and CD4 splenic effector memory ($CD8^+$ or $CD4^+$ $CD44^{hi}CD62L^-$) and central memory ($CD8^+$ or $CD4^+$ $CD44^{hi}CD62L^+$) cells and total numbers of CD8 or CD4-T cells expressing CD44. (**E**) Representative dot blots of CD44 and CD62L staining of both $CD8^+$ and $CD4^+$ liver and splenic lymphocytes in untreated controls (ECM) and chemically attenuated animals (NCM). (**F**) Percentage CD44 expression by $CD8^+$ and $CD4^+$ T cells in liver in untreated controls (ECM) and chemically attenuated animals (NCM). *Upper histograms* represent $CD8^+$ T cells and *lower histograms* $CD4^+$ T cells, and are single representative samples from whole experimental group. (**G**) Percentage CD44 expression by $CD8^+$ and $CD4^+$ T cells in splenic tissue in untreated controls (ECM) and chemically attenuated animals (NCM). *Upper histograms* represent $CD8^+$ T cells and *lower histograms* $CD4^+$ T cells, and are single representative samples from whole experimental group. $^*p < 0.05$, $^{**}p < 0.01$.

after CAT is marked by the early activation of the host immune system.

Animals subjected to CAT exhibited a decrease in T effector cells, T cell activation marker expression, and CD8$^+$CD11c$^+$ dendritic cell numbers at day 8 postinfection

Host immunopathogenesis diverged significantly from ECM mice at the fulminant stage of disease. At days 8–9 postinfection, NCM mice showed a decrease in splenic CD4$^+$CD44^{hi}CD62L$^-$ T effector subsets, and a decrease in expression of both CD69 and CD25 activation markers in both splenic CD8$^+$ and CD4$^+$ T cells (Supplemental Fig. 3E and 3F). T cell activation in ECM occurred in response to a systemic Th1 environment and Ag presentation by CD11c$^+$ dendritic cells (DCs) (41, 42). We observed a lower number of CD11c^{high}CD8$^+$ DCs in our NCM model in liver and a pronounced decrease in spleen at day 8 postinfection (Fig. 6).

Adoptive transfer of splenocytes from animals subjected to CAT leads to 70% protection against ECM and is ablated upon depletion of CD8$^+$ T cells, but not CD25$^+$ or CD4$^+$ T cells from late-phase infection

To investigate the transferability of the early immune environment in NCM, we performed an adoptive transfer of 2×10^7 liver-derived lymphocytes at 48 h after sporozoite inoculation into naive

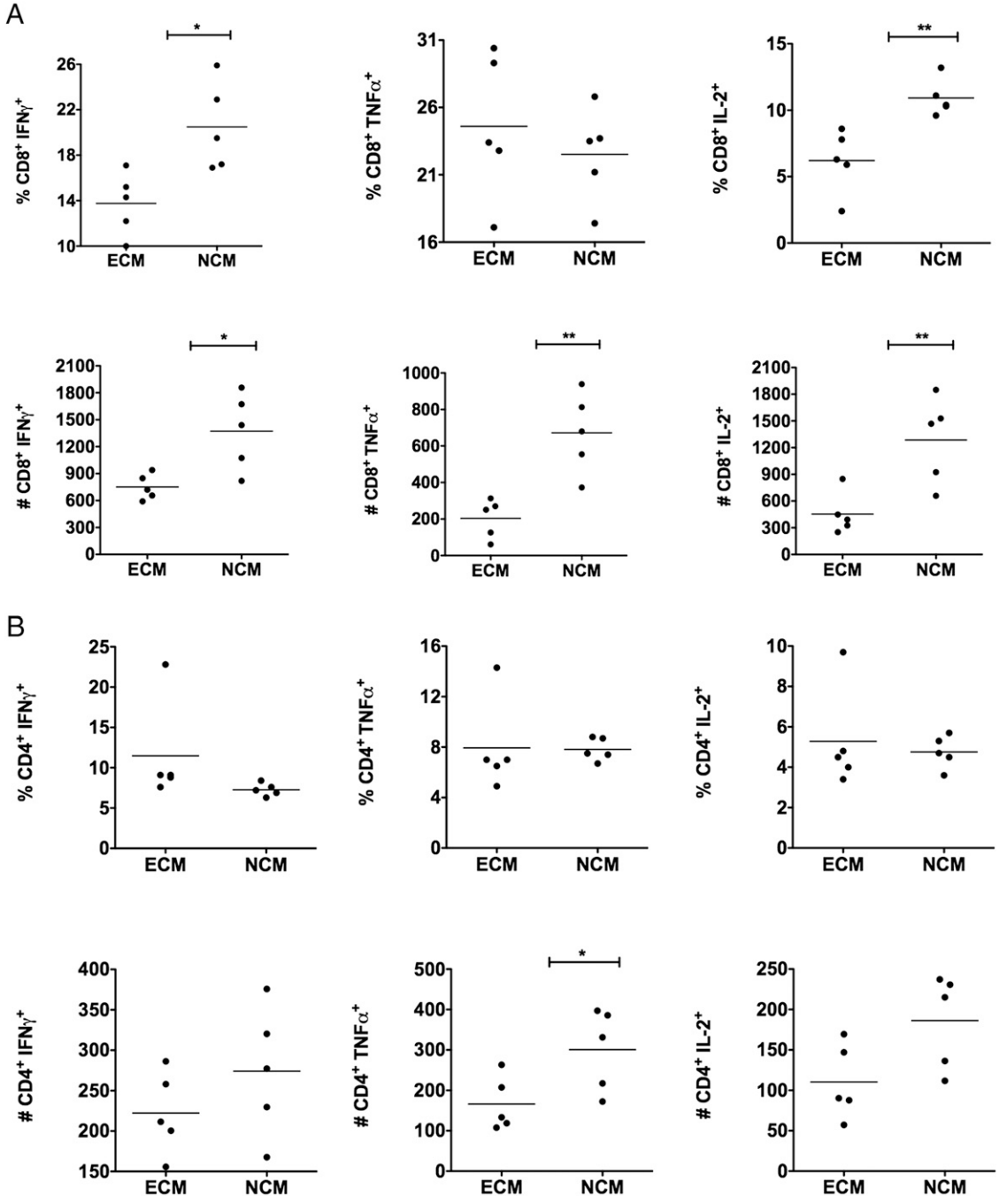

FIGURE 5. Animals subjected to CAT feature increased cytokine expression by CD8$^+$ T cells and increased TNF-α expression by CD4$^+$ T at day 4 postinfection. Animals (groups of 5) were assigned to ECM and NCM groups as described, infected with 10,000 *P. berghei* ANKA sporozoites, and sacrificed at day 4 postinfection. Livers were harvested and lymphocytes isolated and cultured ex vivo with PMA/Ionomycin and brefeldin A. (**A**) Cells were stained for CD8 and IFN-γ, TNF-α, and IL-2. (**B**) Cells were stained for CD4 and IFN-γ, TNF-α, and IL-2. *$p < 0.05$, **$p < 0.01$.

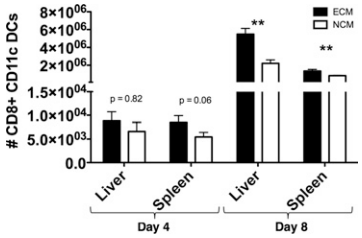

FIGURE 6. Animals subjected to CAT display fewer $CD8^+CD11c^+$ DCs at day 8. Animals (groups of 5) were assigned to ECM and NCM groups as described, and infected with 10,000 *P. berghei* ANKA sporozoites, and sacrificed at days 4 and 8 postinfection. Liver and spleen were harvested, and lymphocytes isolated and stained for CD8 and CD11c to determine whole number of $CD8^+CD11c^+$ DC population. $^{**}p < 0.01$.

animals, which were challenged with 10,000 *P. berghei* ANKA sporozoites 24 h later. This did not confer any difference in protection between NCM- and ECM-recipient animals. In contrast, adoptive transfer of 2×10^7 whole splenocytes from NCM donors to naive mice led to around 70% protection of mice against cerebral symptoms compared with 0% protection in control animals that received splenocytes from ECM donors (Fig. 7A). Strikingly, this protection could not be conferred if donor NCM mice were depleted of $CD8^+$ T cells (Fig. 7A). We therefore assume that NCM protection is essentially mediated by splenic $CD8^+$ T cells, as part of a systemic modulation of the early host immune response. Quantification of parasite liver load by qRT-PCR at 42 h postinfection in adoptive transfer recipients revealed no significant difference between adoptive transfer recipients from NCM and ECM donors, respectively (Supplemental Fig. 4A), indicating that adoptively transferred splenocytes do not have a cytolytic effect on infected hepatocytes. Because it has been shown that $CD4^+$ T cells are required for the induction of cerebral pathology in C57BL/6 mice and their early depletion leads to protection from cerebral pathology (43, 44), we administered CD4-depleting Ab to animals subjected to CAT from day 6 postinfection to determine the role of $CD4^+$ T cells at late infection. All animals were protected from cerebral pathology. Similarly, depletion of CD25 from early infection did not alter the NCM phenotype (Supplemental Fig. 4B and 4C).

Protection arising from CAT cannot be elicited in mice deficient of IL-10, indicating that NCM protection may depend upon IL-10

Given the presumed downregulation of the Th1 response during fulminant infection in CAT mice, because of the absence of cerebral pathology, we investigated the role of the anti-inflammatory cytokine IL-10. IL-10 is a master regulator of immunity to malaria and is important in ECM immunopathology, controlling Th1 responses (45, 46). Because protection by CAT is associated with stronger proinflammatory responses at earlier time points in contrast with ECM controls, which decrease at later infection, we investigated the role of IL-10 in the NCM model. We subjected IL-$10^{tm1Cgrn}$ knockout mice and WT mice treated with anti–IL-10R Ab to CAT and subsequently challenged with 10,000 *P. berghei* ANKA sporozoites. Animals had ECM pathology and died at days 10–12, indicating the requirement of IL-10 in NCM (Fig. 7B). We next injected chemically attenuated mice with IL-10R Ab at day 5 postinfection, and protection was still abrogated (Fig. 7C). This suggests that the protective role of IL-10 in NCM is stage specific and mediated from the later stages, not the pre-erythrocytic stage (Fig. 8). To determine whether protection could be conferred to IL-10 knockout mice by adoptive transfer of splenocytes from chemically attenuated wild-type mice, we subjected IL-10 knockout mice to adoptive transfer as described earlier. All animals succumbed to cerebral pathology (Supplemental Fig. 4D).

Discussion

In most studies focusing on murine cerebral immunopathogenesis, the pre-erythrocytic and early erythrocytic stages have been largely overlooked. In contrast, our study uncovers a previously unelucidated role for the pre-erythrocytic stage in ECM and emerging T cell responses. Classically, upon infection of erythrocytes and clearance in the spleen, the host undergoes a Th1 response that involves the production of proinflammatory cytokines and the recruitment of innate immune cells such as monocytes and neutrophils and their chemotaxis to the brain microvasculature (47–49). A diverse range of cytokines, especially the proinflammatory cytokine IFN-γ, also increases expression of adhesion molecules such as ICAM-1 and LFA-1 (50, 51). DCs capture and present Ags during the rupture of pRBCs and their clearance in the spleen. This, together with the overriding Th1 environment and costimulatory signals provided by adhesion molecules (52), causes T lymphocytes to become activated and migrate via chemotaxis to the brain microvasculature. It is this adaptive response, and T cell activation, that occurs in late blood-stage infection that leads to BBB damage and pathology.

Some experimental ECM models with "unnaturally early" IFN-γ responses have been associated with protection from ECM (18, 19), where inflammatory responses may diverge from their normal role of mediating splenic T cell activation and the development of pathology during the fulminant stage of disease (3). We believe that chemical attenuation in the NCM model causes protection via a similar dynamics (Fig. 8). The pre-erythrocytic parasite development following CAT is marked by a significant

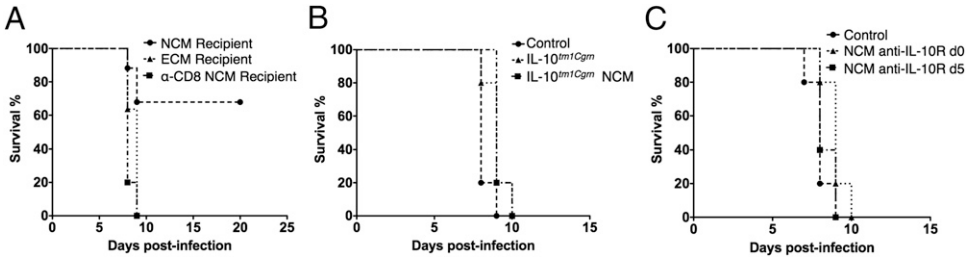

FIGURE 7. The NCM phenotype can be adoptively transferred and relies on $CD8^+$ T cells and IL-10. (**A**) NCM and ECM mice were either depleted or not of their $CD8^+$ T cells, infected with 10,000 *P. berghei* ANKA sporozoites, and sacrificed at day 2 postinfection. Splenic lymphocytes from the depleted and undepleted donor groups were isolated, pooled, and adoptively transferred into recipient mice (groups of 5). Recipient mice were infected with 10,000 *P. berghei* ANKA sporozoites 24 h posttransfer and survival tracked (experiment performed in triplicates). (**B**) IL-$10^{tm1Cgrn}$ knockout mice were subjected to CAT (NCM), infected with 10,000 *P. berghei* ANKA sporozoites, and survival tracked (experiment performed in triplicates). (**C**) NCM mice were administered anti–IL-10R Ab i.p. at either day 0 or 5 postinfection and compared with control mice, infected with 10,000 *P. berghei* ANKA sporozoites, and survival was tracked (experiment performed in duplicates).

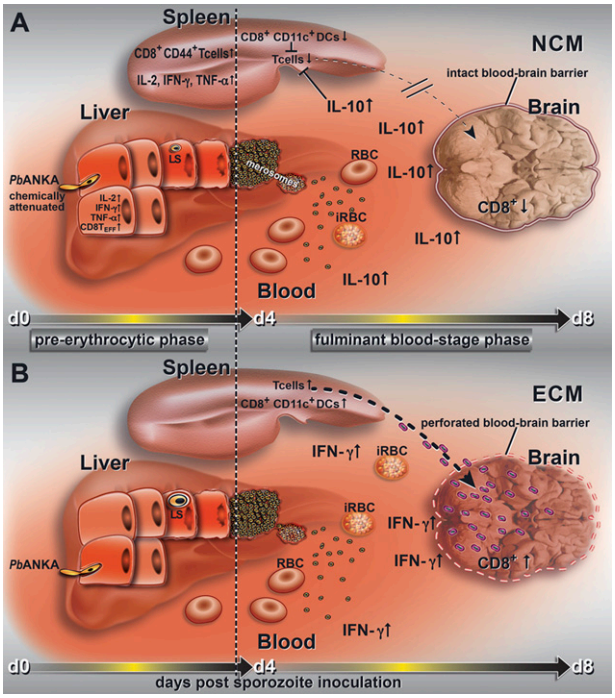

FIGURE 8. A hypothetical schema detailing how CAT affects malaria immunopathogenesis. (**A**) CAT leads to NCM outcome. After sporozoite invasion, chemical attenuation of the parasite causes prolonged pre-erythrocytic development in the liver before the onset of blood-stage infection. Attenuated development at this early time point causes an increase in T effector cells at the liver and production of proinflammatory cytokines. These activated T cells migrate to the spleen where there is an associated increase in T effector cells and Th1 responses before the release of merosomes and rupture of infected erythrocytes. At the point of blood-stage infection, the delicate balance required for ECM immunopathology is disrupted. Reduced numbers of $CD8^+CD11c^+$ DCs in the spleen are associated with decreased phagocytosis of parasite moieties, which, in turn, leads to decreased priming of lymphocytes. Systemic inflammation is therefore reduced at the fulminant stage of infection, leading to reduced endothelial cell activation in the brain, reduced binding of infected erythrocytes to endothelial receptors, and reduced migration of lymphocytes from the spleen to the brain microvasculature. This, in turn, reduces leukocyte and parasite sequestration and prevents damage to the BBB and associated cerebral pathology. (**B**) Absence of CAT leads to ECM outcome. After sporozoite invasion, parasites undergo pre-erythrocytic development in the liver before the onset of blood-stage infection. No significant protective proinflammatory response occurs at either liver or spleen at the pre-erythrocytic stage. At blood-stage infection, increasing blood-stage parasitemia and rupture of infected erythrocytes is associated with phagocytosis of parasite moieties by splenic $CD8^+CD11c^+$ DCs, which exogenously process Ag via MHCI, prime and activate lymphocytes, and cause systemic inflammation, associated with proinflammatory cytokines such as IFN-γ. Systemic inflammation increases endothelial activation in the brain, increased binding of infected erythrocytes to endothelial receptors and increased migration of lymphocytes from the spleen to the brain microvasculature in response to chemokines. This leukocyte and parasite sequestration damages the BBB and leads to cerebral pathology, possibly through Ag-specific T cell cytotoxicity, via MHCI-restricted presentation of parasite-derived Ag on endothelial cells; hemorrhaging, coma, and death result.

reduction in liver burden at 42 h postinfection and a decreased parasite biomass in the host from 72 to 96 h postinfection following merosome egress. By PCR analysis, all animals subjected to CAT became blood-stage–positive some 12 h after the ECM controls, at 96 and 84 h postinfection, respectively. The disparity in the apparent onset of blood parasitemia between the two experimental approaches may be because of the insufficiency of PCR to amplify parasite material from a low volume of blood isolated from a mouse with submicroscopic parasitemia. Interestingly, liver-stage development appears to be essential for protection from cerebral pathology, because both low- and high-dose challenge of pRBCs following CAT failed to protect from ECM.

As revealed by immunofluorescence microscopy, the number of liver-stage parasites does not differ in protected animals. However, most liver stages in protected animals are considerably less developed than in nonprotected controls, whereas only a small number of EEFs appears to show normal development, suggesting that they may have escaped attenuation marked by an unchanged parasitophorous vacuolar membrane. This attenuated growth correlates with an equally idiosyncratic early immune response. Indeed, following CAT and sporozoite challenge, attenuated parasite development induces T cell activation within both liver and spleen, and increased IFN-γ, TNF-α, and IL-2 production by $CD8^+$ lymphocytes at an earlier time point than in a normal ECM infection. This early peak appears to cause modulation of later inflammatory immunopathogenesis in the host, during the phase where splenic T cells would normally become activated and migrate to the brain at the crucial time point between days 8 and 10 postinfection (days 4–6 postblood infection) (3). This may be similar to other experimental ECM models in which early IFN-γ production was associated with protection (18, 19). Early NCM immunopathogenesis following CAT is marked by the early activation of the host immune system, possibly by isopentaquine-killed parasites, in turn leading to increased accumulation of splenic T effector cells and a pronounced intrahepatic and splenic Th1-environment. NCM hosts display decreased $CD11c^{hi}CD8^+$ DC numbers, downregulation of T cell activation, no cerebral infiltration, and a complete absence of cerebral pathology. The connection between $CD11c^{hi}CD8^+$ DCs and ECM is well established. Parasites associate with these DCs, which capture dying cells and exogenously process Ag for cross-presentation via MHCI (53). They have been shown to prime naive $CD8^+$ T cell proliferation and CTL effector functions (54) with the induction of specific $CD8^+$ T cell responses abrogated in their absence (55). Recent work suggests $CD11c^{high}CD8^+$ DCs are responsible for ECM immunopathogenesis (42). Although we did not test the capacity for Ag presentation in DCs, we observed a decreased number and concurrent reduction in T cell activation at the fulminant stage of infection, a component of the overall downregulation in Th1 responses. We speculated that this downregulation may be mediated by the anti-inflammatory cytokine IL-10 during the fulminant stage of disease in a response that we hypothesize represents the host bringing its early proinflammatory response under control, at the stage where T cell priming and/or chemotaxis to the brain would occur. IL-10 plays an essential role in ECM immunopathology that can both impede pathogen clearance and ameliorate immunopathology (45, 46). Furthermore, it has been demonstrated that neutralization of IL-10 leads to ECM symptoms in otherwise resistant mice (56). Although we did not observe an increased level of IL-10 protein in mice subjected to CAT, we were unable to induce NCM protection in those lacking the cytokine, perhaps due in part to increased ECM pathology in its absence. This strongly indicates the requirement of IL-10 for the NCM phenotype. Because regulatory T cells are associated with the production of IL-10 and the limitation of inflammatory pathology (57) and have been associated with protection from ECM (58), we speculated that they might be responsible for the production of IL-10 in the NCM model or otherwise mediate T cell responses. Although depletion of CD25 had no effect on the protective phenotype (Supplemental Fig. 4B), some reports have indicated that $CD25^+$ cells are required for development of cerebral pathology in susceptible mice (59, 60), so we cannot exclude their role in NCM, and the source of IL-10 remains unknown. Recent literature reports an IL-10–producing $CD4^+CD25^-Foxp3^-$ regulatory

T cell subset associated with the modulation of pathology in *Plasmodium yoelii* (61), although depletion of $CD4^+$ cells from day 6 postinfection had no effect on the protective phenotype observed in NCM animals.

The early inflammatory peak in the NCM phenotype caused by CAT appears to be largely caused by $CD8^+$ T cells, including the effector memory subset, because adoptive transfer of splenocytes from mice subjected to CAT cannot confer protection to naive animals in their absence. Adoptive transfer into IL-$10^{tm1Cgrn}$ knockout mice was not able to confer protection, perhaps unsurprisingly, because NCM protection is dependent upon IL-10. Although we cannot comment as to epitope specificity of these $CD8^+$ T cells, we assume that they are specific to pre-erythrocytic parasite Ag. The Ag specificity of T cells that migrate to the brain in ECM is still mostly undescribed, although a recent publication identified one conserved CD8 epitope cross-presented by the brain microvessels (5). Although it is attractive to speculate that a shared antigenic repertoire may exist between the parasitized hepatocyte and the infected erythrocyte, and is displayed via MHCI on the cytokine-activated brain endothelial cell (62), it is conceivable that $CD8^+$ T cell–mediated protection leading to NCM is not restricted to any one particular Ag. Indeed, it is possible that early T cell priming, regardless of Ag, causes a more generalized, systemic downregulation of the Th1 response, Ag presentation, and T cell activation where and when it matters, at the onset of fulminant disease. Furthermore, it is possible that a reduced parasite load in the liver due to CAT induces the priming of differential $CD8^+$ specificities to those that mediate ECM. Follow-up experiments will isolate protective $CD8^+$ T cells and determine their precise epitope specificity, longevity, and effect after adoptive transfer.

Quantification of liver burden after adoptive transfer and sporozoite infection revealed no significant difference between recipients of adoptively transferred splenocytes from protected animals and ECM control animals, indicating that adoptively transferred $CD8^+$ T cells are not engaged in cytolytic parasite killing. However, a recent study in *P. yoelii* reported that adoptive transfer of splenic and hepatic lymphocytes renders $CD8^+$ T cells immotile and unable to make contact with *Plasmodium*-infected hepatocytes (63). Thus, we cannot exclude that parasite killing by $CD8^+$ T cells does occur in animals subjected to CAT. After adoptive transfer, the inability of immobilized $CD8^+$ T cells to make contact with infected hepatocytes may render them reliant on soluble mediators to modulate cerebral immunopathogenesis. This may explain why adoptive transfer does not lead to 100% protection. Our work has far-reaching implications in dissecting the complex sequence of interrelated events that form the immunological basis of HCM pathology, thought to begin with pRBC sequestration or rupture (3). We suggest a role for the early intrahepatic host immune responses that can alter the course of downstream-systemic immunopathogenesis. The liver is an immunoprivileged organ typified by tolerogenic, limited T cell responses (64). We suggest that liver tolerance may explain why such potentially protective pre-erythrocytic responses do not naturally occur in HCM. The decrease in severe pathology, including cerebral symptoms, and yet onset of blood infection in the RTS,S vaccine trials are so far unexplained. RTS,S consists of sequences from the C-terminal region of the CS protein (65) and is designed to produce a pre-erythrocytic T cell response directed against the infected liver. It is conceivable that this provokes T cell responses akin to those in the NCM model, and we hypothesize that these data may provide a mechanistic basis for the unexplained decrease in severe and cerebral pathology observed in the RTS,S malaria vaccination trials and other pre-erythrocytic malaria interventions (10, 17).

Acknowledgments

We thank Jennifer Schahn and Miriam Ester for mosquito breeding, Aina Martin Valls, Jessica Kehrer, and Evelyn Exner for expert technical assistance, Yves Cully for illustrations, Bianca Schneider, Roland Frank, Britta Nyboer, Hans-Willi Mittruecker, and Beatrix Schumak for critical discussions and helpful comments on the manuscript, Melanie Lödige and Eleonora Paulsen for synthesizing the isopentaquine compound, Michael Meister and Johannes Pfeil for assistance with bioluminescence analysis, and Beatrix Schumak for kindly providing IL-$10^{tm1Cgrn}$ knockout mice and anti-CD4–depleting Ab clone GK1.5 purified from hybridoma culture. We are grateful to the Forschungszentrum Borstel for allowing us to perform cytokine bead array experiments.

Disclosures

The authors have no financial conflicts of interest.

References

1. Haldar, K., S. C. Murphy, D. A. Milner, and T. E. Taylor. 2007. Malaria: mechanisms of erythrocytic infection and pathological correlates of severe disease. *Annu. Rev. Pathol.* 2: 217–249.
2. Patnaik, J. K., B. S. Das, S. K. Mishra, S. Mohanty, S. K. Satpathy, and D. Mohanty. 1994. Vascular clogging, mononuclear cell margination, and enhanced vascular permeability in the pathogenesis of human cerebral malaria. *Am. J. Trop. Med. Hyg.* 51: 642–647.
3. de Souza, J. B., J. C. Hafalla, E. M. Riley, and K. N. Couper. 2010. Cerebral malaria: why experimental murine models are required to understand the pathogenesis of disease. *Parasitology* 137: 755–772.
4. Baptista, F. G., A. Pamplona, A. C. Pena, M. M. Mota, S. Pied, and A. M. Vigário. 2010. Accumulation of *Plasmodium* berghei-infected red blood cells in the brain is crucial for the development of cerebral malaria in mice. *Infect. Immun.* 78: 4033–4039.
5. Howland, S. W., C. M. Poh, S. Y. Gun, C. Claser, B. Malleret, N. Shastri, F. Ginhoux, G. M. Grotenbreg, and L. Rénia. 2013. Brain microvessel cross-presentation is a hallmark of experimental cerebral malaria. *EMBO Mol. Med.* 5: 916–931.
6. Miyakoda, M., D. Kimura, M. Yuda, Y. Chinzei, Y. Shibata, K. Honma, and K. Yui. 2008. Malaria-specific and nonspecific activation of CD8+ T cells during blood stage of *Plasmodium* berghei infection. *J. Immunol.* 181: 1420–1428.
7. Engwerda, C., E. Belnoue, A. C. Grüner, and L. Rénia. 2005. Experimental models of cerebral malaria. *Curr. Top. Microbiol. Immunol.* 297: 103–143.
8. de Souza, J. B., and E. M. Riley. 2002. Cerebral malaria: the contribution of studies in animal models to our understanding of immunopathogenesis. *Microbes Infect.* 4: 291–300.
9. Pombo, D. J., G. Lawrence, C. Hirunpetcharat, C. Rzepczyk, M. Bryden, N. Cloonan, K. Anderson, Y. Mahakunkijcharoen, L. B. Martin, D. Wilson, et al. 2002. Immunity to malaria after administration of ultra-low doses of red cells infected with *Plasmodium falciparum.* *Lancet* 360: 610–617.
10. Genton, B., I. Betuela, I. Felger, F. Al-Yaman, R. F. Anders, A. Saul, L. Rare, M. Baisor, K. Lorry, G. V. Brown, et al. 2002. A recombinant blood-stage malaria vaccine reduces *Plasmodium falciparum* density and exerts selective pressure on parasite populations in a phase 1-2b trial in Papua New Guinea. *J. Infect. Dis.* 185: 820–827.
11. Belnoue, E., F. T. Costa, T. Frankenberg, A. M. Vigário, T. Voza, N. Leroy, M. M. Rodrigues, I. Landau, G. Snounou, and L. Rénia. 2004. Protective T cell immunity against malaria liver stage after vaccination with live sporozoites under chloroquine treatment. *J. Immunol.* 172: 2487–2495.
12. Mueller, A. K., M. Labaied, S. H. Kappe, and K. Matuschewski. 2005. Genetically modified *Plasmodium* parasites as a protective experimental malaria vaccine. *Nature* 433: 164–167.
13. Nussenzweig, R. S., J. Vanderberg, H. Most, and C. Orton. 1967. Protective immunity produced by the injection of x-irradiated sporozoites of plasmodium berghei. *Nature* 216: 160–162.
14. Agnandji, S. T., B. Lell, J. F. Fernandes, B. P. Abossolo, B. G. Methogo, A. L. Kabwende, A. A. Adegnika, B. Mordmüller, S. Issifou, P. G. Kremsner, et al; RTS,S Clinical Trials Partnership. 2012. A phase 3 trial of RTS,S/AS01 malaria vaccine in African infants. *N. Engl. J. Med.* 367: 2284–2295.
15. Alonso, P. L., J. Sacarlal, J. J. Aponte, A. Leach, E. Macete, J. Milman, I. Mandomando, B. Spiessens, C. Guinovart, M. Espasa, et al. 2004. Efficacy of the RTS,S/AS02A vaccine against *Plasmodium falciparum* infection and disease in young African children: randomised controlled trial. *Lancet* 364: 1411–1420.
16. Bejon, P., L. Andrews, R. F. Andersen, S. Dunachie, D. Webster, M. Walther, S. C. Gilbert, T. Peto, and A. V. Hill. 2005. Calculation of liver-to-blood inocula, parasite growth rates, and preerythrocytic vaccine efficacy, from serial quantitative polymerase chain reaction studies of volunteers challenged with malaria sporozoites. *J. Infect. Dis.* 191: 619–626.
17. Haussig, J. M., K. Matuschewski, and T. W. Kooij. 2011. Inactivation of a *Plasmodium* apicoplast protein attenuates formation of liver merozoites. *Mol. Microbiol.* 81: 1511–1525.
18. Mitchell, A. J., A. M. Hansen, L. Hee, H. J. Ball, S. M. Potter, J. C. Walker, and N. H. Hunt. 2005. Early cytokine production is associated with protection from murine cerebral malaria. *Infect. Immun.* 73: 5645–5653.

19. Gerald, N. J., V. Majam, B. Mahajan, Y. Kozakai, and S. Kumar. 2011. Protection from experimental cerebral malaria with a single dose of radiation-attenuated, blood-stage *Plasmodium* berghei parasites. *PLoS ONE* 6: e24398. Available at: http://journals.plos.org/plosone/article?id=10.1371/journal.pone.0024398.
20. Janse, C. J., B. Franke-Fayard, G. R. Mair, J. Ramesar, C. Thiel, S. Engelmann, K. Matuschewski, G. J. van Gemert, R. W. Sauerwein, and A. P. Waters. 2006. High efficiency transfection of *Plasmodium* berghei facilitates novel selection procedures. *Mol. Biochem. Parasitol.* 145: 60–70.
21. Carroll, R. W., M. S. Wainwright, K. Y. Kim, T. Kidambi, N. D. Gómez, T. Taylor, and K. Haldar. 2010. A rapid murine coma and behavior scale for quantitative assessment of murine cerebral malaria. *PLoS ONE* 5: 5.
22. Schmidt, K. E., B. Schumak, S. Specht, B. Dubben, A. Limmer, and A. Hoerauf. 2011. Induction of pro-inflammatory mediators in *Plasmodium* berghei infected BALB/c mice breaks blood-brain-barrier and leads to cerebral malaria in an IL-12 dependent manner. *Microbes Infect.* 13: 828–836.
23. Friesen, J., O. Silvie, E. D. Putrianti, J. C. Hafalla, K. Matuschewski, and S. Borrmann. 2010. Natural immunization against malaria: causal prophylaxis with antibiotics. *Sci. Transl. Med.* 2: 40ra49.
24. Ploemen, I. H., M. Prudêncio, B. G. Douradinha, J. Ramesar, J. Fonager, G. J. van Gemert, A. J. Luty, C. C. Hermsen, R. W. Sauerwein, F. G. Baptista, et al. 2009. Visualisation and quantitative analysis of the rodent malaria liver stage by real time imaging. *PLoS ONE* 4: e7881. Available at: http://journals.plos.org/plosone/article?id=10.1371/journal.pone.0007881.
25. Prudêncio, M., M. M. Mota, and A. M. Mendes. 2011. A toolbox to study liver stage malaria. *Trends Parasitol.* 27: 565–574.
26. Zar, J. H. 1984. *Biostatistical analysis.* Prentice-Hall, Englewood Cliffs, London.
27. Cooper, W. C. 1949. Summary of antimalarial drugs. *J. Am. Pharm. Assoc. Am. Pharm. Assoc. (Baltim).* 10: 552–556.
28. Elderfield, R. C., and S. J. Gensler, et al. 1946. Alkylaminoalkyl derivatives of 8-aminoquinoline. *J. Am. Chem. Soc.* 68: 1524–1529.
29. Schmidt, L. H. 1983. Relationships between chemical structures of 8-aminoquinolines and their capacities for radical cure of infections with *Plasmodium* cynomolgi in rhesus monkeys. *Antimicrob. Agents Chemother.* 24: 615–652.
30. Hill, D. R., J. K. Baird, M. E. Parise, L. S. Lewis, E. T. Ryan, and A. J. Magill. 2006. Primaquine: report from CDC expert meeting on malaria chemoprophylaxis I. *Am. J. Trop. Med. Hyg.* 75: 402–415.
31. Franke-Fayard, B., A. P. Waters, and C. J. Janse. 2006. Real-time in vivo imaging of transgenic bioluminescent blood stages of rodent malaria parasites in mice. *Nat. Protoc.* 1: 476–485.
32. Prudêncio, M., A. Rodriguez, and M. M. Mota. 2006. The silent path to thousands of merozoites: the *Plasmodium* liver stage. *Nat. Rev. Microbiol.* 4: 849–856.
33. Hearn, J., N. Rayment, D. N. Landon, D. R. Katz, and J. B. de Souza. 2000. Immunopathology of cerebral malaria: morphological evidence of parasite sequestration in murine brain microvasculature. *Infect. Immun.* 68: 5364–5376.
34. Jennings, V. M., A. A. Lal, and R. L. Hunter. 1998. Evidence for multiple pathologic and protective mechanisms of murine cerebral malaria. *Infect. Immun.* 66: 5972–5979.
35. Neill, A. L., and N. H. Hunt. 1992. Pathology of fatal and resolving *Plasmodium* berghei cerebral malaria in mice. *Parasitology* 105: 165–175.
36. Polder, T. W., W. M. Eling, J. H. Curfs, C. R. Jerusalem, and M. Wijers-Rouw. 1992. Ultrastructural changes in the blood-brain barrier of mice infected with *Plasmodium* berghei. *Acta Leiden.* 60: 31–46.
37. Rest, J. R. 1982. Cerebral malaria in inbred mice. I. A new model and its pathology. *Trans. R. Soc. Trop. Med. Hyg.* 76: 410–415.
38. Belnoue, E., M. Kayibanda, A. M. Vigario, J. C. Deschemin, N. van Rooijen, M. Viguier, G. Snounou, and L. Rénia. 2002. On the pathogenic role of brain-sequestered alphabeta CD8+ T cells in experimental cerebral malaria. *J. Immunol.* 169: 6369–6375.
39. Amante, F. H., A. Haque, A. C. Stanley, Fde. L. Rivera, L. M. Randall, Y. A. Wilson, G. Yeo, C. Pieper, B. S. Crabb, T. F. de Koning-Ward, et al. 2010. Immune-mediated mechanisms of parasite tissue sequestration during experimental cerebral malaria. *J. Immunol.* 185: 3632–3642.
40. Chao, K. H., M. Y. Wu, J. H. Yang, S. U. Chen, Y. S. Yang, and H. N. Ho. 2002. Expression of the interleukin-2 receptor alpha (CD25) is selectively decreased on decidual CD4+ and CD8+ T lymphocytes in normal pregnancies. *Mol. Hum. Reprod.* 8: 667–673.
41. deWalick, S., F. H. Amante, K. A. McSweeney, L. M. Randall, A. C. Stanley, A. Haque, R. D. Kuns, K. P. MacDonald, G. R. Hill, and C. R. Engwerda. 2007. Cutting edge: conventional dendritic cells are the critical APC required for the induction of experimental cerebral malaria. *J. Immunol.* 178: 6033–6037.
42. Piva, L., P. Tetlak, C. Claser, K. Karjalainen, L. Renia, and C. Ruedl. 2012. Cutting edge: Clec9A+ dendritic cells mediate the development of experimental cerebral malaria. *J. Immunol.* 189: 1128–1132.
43. Yañez, D. M., D. D. Manning, A. J. Cooley, W. P. Weidanz, and H. C. van der Heyde. 1996. Participation of lymphocyte subpopulations in the pathogenesis of experimental murine cerebral malaria. *J. Immunol.* 157: 1620–1624.
44. Yañez, D. M., J. Batchelder, H. C. van der Heyde, D. D. Manning, and W. P. Weidanz. 1999. Gamma delta T-cell function in pathogenesis of cerebral malaria in mice infected with *Plasmodium* berghei ANKA. *Infect. Immun.* 67: 446–448.
45. Couper, K. N., D. G. Blount, and E. M. Riley. 2008. IL-10: the master regulator of immunity to infection. *J. Immunol.* 180: 5771–5777.
46. Langhorne, J., F. R. Albano, M. Hensmann, L. Sanni, E. Cadman, C. Voisine, and A. M. Sponaas. 2004. Dendritic cells, pro-inflammatory responses, and antigen presentation in a rodent malaria infection. *Immunol. Rev.* 201: 35–47.
47. Grau, G. E., L. F. Fajardo, P. F. Piguet, B. Allet, P. H. Lambert, and P. Vassalli. 1987. Tumor necrosis factor (cachectin) as an essential mediator in murine cerebral malaria. *Science* 237: 1210–1212.
48. Medana, I. M., N. H. Hunt, and G. Chaudhri. 1997. Tumor necrosis factor-alpha expression in the brain during fatal murine cerebral malaria: evidence for production by microglia and astrocytes. *Am. J. Pathol.* 150: 1473–1486.
49. Pais, T. F., and S. Chatterjee. 2005. Brain macrophage activation in murine cerebral malaria precedes accumulation of leukocytes and CD8+ T cell proliferation. *J. Neuroimmunol.* 163: 73–83.
50. Amani, V., A. M. Vigário, E. Belnoue, M. Marussig, L. Fonseca, D. Mazier, and L. Rénia. 2000. Involvement of IFN-gamma receptor-medicated signaling in pathology and anti-malarial immunity induced by *Plasmodium* berghei infection. *Eur. J. Immunol.* 30: 1646–1655.
51. Bauer, P. R., H. C. Van Der Heyde, G. Sun, R. D. Specian, and D. N. Granger. 2002. Regulation of endothelial cell adhesion molecule expression in an experimental model of cerebral malaria. *Microcirculation* 9: 463–470.
52. Sharpe, A. H. 1995. Analysis of lymphocyte costimulation in vivo using transgenic and 'knockout' mice. *Curr. Opin. Immunol.* 7: 389–395.
53. den Haan, J. M., S. M. Lehar, and M. J. Bevan. 2000. CD8(+) but not CD8(-) dendritic cells cross-prime cytotoxic T cells in vivo. *J. Exp. Med.* 192: 1685–1696.
54. Lundie, R. J., T. F. de Koning-Ward, G. M. Davey, C. Q. Nie, D. S. Hansen, L. S. Lau, J. D. Mintern, G. T. Belz, L. Schofield, F. R. Carbone, et al. 2008. Blood-stage *Plasmodium* infection induces CD8+ T lymphocytes to parasite-expressed antigens, largely regulated by CD8alpha+ dendritic cells. *Proc. Natl. Acad. Sci. USA* 105: 14509–14514.
55. Jung, S., D. Unutmaz, P. Wong, G. Sano, K. De los Santos, T. Sparwasser, S. Wu, S. Vuthoori, K. Ko, F. Zavala, et al. 2002. In vivo depletion of CD11c+ dendritic cells abrogates priming of CD8+ T cells by exogenous cell-associated antigens. *Immunity* 17: 211–220.
56. Kossodo, S., C. Monso, P. Juillard, T. Velu, M. Goldman, and G. E. Grau. 1997. Interleukin-10 modulates susceptibility in experimental cerebral malaria. *Immunology* 91: 536–540.
57. Rubtsov, Y. P., J. P. Rasmussen, E. Y. Chi, J. Fontenot, L. Castelli, X. Ye, P. Treuting, L. Siewe, A. Roers, W. R. Henderson, Jr., et al. 2008. Regulatory T cell-derived interleukin-10 limits inflammation at environmental interfaces. *Immunity* 28: 546–558.
58. Haque, A., S. E. Best, F. H. Amante, S. Mustafah, L. Desbarrieres, F. de Labastida, T. Sparwasser, G. R. Hill, and C. R. Engwerda. 2010. CD4+ natural regulatory T cells prevent experimental cerebral malaria via CTLA-4 when expanded in vivo. *PLoS Pathog.* 6: e1001221. Available at: http://journals.plos.org/plospathogens/article?id=10.1371/journal.ppat.1001221.
59. Amante, F. H., A. C. Stanley, L. M. Randall, Y. Zhou, A. Haque, K. McSweeney, A. P. Waters, C. J. Janse, M. F. Good, G. R. Hill, and C. R. Engwerda. 2007. A role for natural regulatory T cells in the pathogenesis of experimental cerebral malaria. *Am. J. Pathol.* 171: 548–559.
60. Vigário, A. M., O. Gorgette, H. C. Dujardin, T. Cruz, P. A. Cazenave, A. Six, A. Bandeira, and S. Pied. 2007. Regulatory CD4+ CD25+ Foxp3+ T cells expand during experimental *Plasmodium* infection but do not prevent cerebral malaria. *Int. J. Parasitol.* 37: 963–973.
61. Couper, K. N., D. G. Blount, M. S. Wilson, J. C. Hafalla, Y. Belkaid, M. Kamanaka, R. A. Flavell, J. B. de Souza, and E. M. Riley. 2008. IL-10 from CD4CD25Foxp3CD127 adaptive regulatory T cells modulates parasite clearance and pathology during malaria infection. *PLoS Pathog.* 4: e1000004. Available at: http://journals.plos.org/plospathogens/article?id=10.1371/journal.ppat.1000004.
62. Rénia, L., S. M. Potter, M. Mauduit, D. S. Rosa, M. Kayibanda, J. C. Deschemin, G. Snounou, and A. C. Grüner. 2006. Pathogenic T cells in cerebral malaria. *Int. J. Parasitol.* 36: 547–554.
63. Cabrera, M., L. L. Pewe, J. T. Harty, and U. Frevert. 2013. In vivo CD8+ T cell dynamics in the liver of *Plasmodium* yoelii immunized and infected mice. *PLoS ONE* 8: e70842. Available at: http://journals.plos.org/plosone/article?id=10.1371/journal.pone.0070842.
64. Crispe, I. N., M. Giannandrea, I. Klein, B. John, B. Sampson, and S. Wuensch. 2006. Cellular and molecular mechanisms of liver tolerance. *Immunol. Rev.* 213: 101–118.
65. Gordon, D. M., T. W. McGovern, U. Krzych, J. C. Cohen, I. Schneider, R. LaChance, D. G. Heppner, G. Yuan, M. Hollingdale, M. Slaoui, et al. 1995. Safety, immunogenicity, and efficacy of a recombinantly produced *Plasmodium falciparum* circumsporozoite protein-hepatitis B surface antigen subunit vaccine. *J. Infect. Dis.* 171: 1576–1585.